Unique fossil preservation in ferruginous Silurian deposits from the Carnic Alps, Italy

Annalisa Ferretti, Barbara Cavalazzi, Maria Giovanna Corriga,
Samuele Desogus, Carlotta Franchini, Daniele Malferrari, Colin Ongari,
Camilla Zocchi & Carlo Corradini

Conodont residues from Silurian calcareous levels exposed in the Rio Tamer area of the Carnic Alps, Italy, have produced three-dimensional fossil skeletal remains that are typically not preserved in organisms with calcareous shells, as such structures dissolve during standard acid laboratory processing. This unique preservation has been facilitated by early precipitation of iron oxides and hydroxides, which replicated the original skeletons. The fossil assemblage is dominated by benthic fauna and includes echinoderms, trilobites, bivalves, ostracods and gastropods, preserved in the form of ferruginous external coatings or internal moulds. These often retain fine details of the original shell structure. The material was characterised by using optical and scanning electron microscopy (SEM), environmental scanning electron microscopy coupled with microanalyses (SEM/ESEM-EDX), X-ray powder diffraction (XRPD) and confocal laser Raman microscopy. The combined results indicate that the skeletal replicas are primarily composed of goethite, chamosite and hematite, with subordinate amount of siderite, birnessite, quartz and amorphous material. Additionally, the presence of carbonaceous material within the coatings suggests a biologically mediated process in crust formation. Overall, the findings from this study highlight the role of microbial activity in triggering unusual and unique fossil preservational pathways. • Key words: taphonomy, Kok Formation, Mt. Cocco, biomineralization, skeletal replicas, hematite, goethite.

Ferretti, A., Cavalazzi, B., Corriga, M.G., Desogus, S., Franchini, C., Malferrari, D., Ongari, C., Zocchi, C. & Corradini, C. 2025. Unique fossil preservation in ferruginous Silurian deposits from the Carnic Alps, Italy. *Bulletin of Geosciences 100*(*4*), 661–676 (8 figures, 2 tables). Czech Geological Survey, Prague. ISSN 1214-1119. Manuscript received March 5, 2025; accepted in revised form September 9, 2025; published online October 26, 2025; issued December 31, 2025.

Annalisa Ferretti, Carlotta Franchini, Daniele Malferrari & Colin Ongari, Department of Chemical and Geological Sciences (DSCG), University of Modena and Reggio Emilia, Via Campi 103, 41125 Modena, Italy • Barbara Cavalazzi, Department of Biological, Geological, and Environmental Sciences (BiGeA), University of Bologna, 40126 Bologna, Italy & Department of Geology, University of Johannesburg, Johannesburg, South Africa • Maria Giovanna Corriga (corresponding author), Samuele Desogus, Camilla Zocchi & Carlo Corradini, Department of Mathematics, Informatics and Geosciences, University of Trieste, Via Weiss 2, 34128 Trieste, Italy; corrigamariagiovanna@gmail.com

In palaeontology, the term ‘exceptional preservation’ is commonly used when fossilization captures easily decomposable parts, such as soft tissues or non-biomineralised fossils, which typically decay rapidly after death and are lost during fossilization. Such extraordinary preservation requires specific burial and/or diagenetic conditions that enable the preservation of carbonaceous materials or their secondarily mineral replication (*e.g.* Briggs 2003). Additionally, the absence of disturbance in bottom sediments – whether from wave action, currents, or benthic fauna – also plays a crucial role (*e.g.* Schwark *et al.* 2009). However, unique fossilizations can also occur when remineralization enables some fossil remains to be documented under contexts that are generally unfavourable for preservation. This is particularly relevant in microfossil extraction techniques that rely on acid digestion (*e.g.* Jarochowska *et al.* 2013) and therefore would normally destroy calcareous hard parts. Depending on the chemical conditions, not only the hosting carbonate rock but also any skeletal shell embedded within – if of the same composition – will be dissolved. For example, when extracting conodonts or other phosphatic/phosphatised skeletal remains from calcareous rocks using acid solution (*e.g.* formic or acetic acid), any calcareous skeletal elements are also removed.

Conodont residues from processed limestone blocks sampled from Silurian deposits of the Rio Tamer area of the eastern Carnic Alps, Italy (Fig. 1) revealed unique three-dimensional fossil bodies preserved as ferruginous external coatings or positive casts of originally calcareous

DOI 10.3140/bull.geosci.1926

organisms, primarily echinoderms, trilobites, bivalves, ostracods and gastropods. Similar ferruginous laminated structures overgrowing specific skeletal fragments in a distinct stromatolitic pattern, have been reported in the Carnic Alps and described in thin sections from the Silurian of the Wolayer area (Ferretti 2005, Brett *et al.* 2012, Ferretti *et al.* 2012, Corriga *et al.* 2021) and the Upper Ordovician of the Cellon section (Ferretti *et al.* 2023a). In these previously reported examples, the structures consist of alternating layers of iron-rich oxides and hydroxides interspersed with calcite bands. The association with carbonaceous matter and fossilised microbial structures indicates that microbial activities played a key role in their formation.

This study aims to analyse the preservation of these three-dimensional ferruginous skeletal replicas from the Tamer area, determine their composition and significance, and propose a formation model. To achieve this, we integrate analyses using optical and scanning electron microscopy (SEM), environmental scanning electron microscopy coupled with microanalyses (ESEM-EDX), X-ray powder diffraction (XRPD), and confocal laser Raman microscopy.

Geological setting

The Palaeozoic of the Carnic Alps is represented by almost completely exposed sequences, documenting ?Cambrian–Lower Ordovician to Upper Permian sedimentary successions with an approximately east–west alignment at the Italian–Austrian border (Ferretti *et al.* 2023b). Although the Palaeozoic successions there have been intensively investigated for over 150 years, the lithostratigraphy of pre-Variscan units has only been formalised recently (Corradini & Suttner 2015) as a result of an international project involving mainly Austrian and Italian scientists.

The Silurian is one of the best-studied intervals, due to the precise biostratigraphic assignment of the Carnic units based primarily on conodonts and graptolites (*e.g.* Walliser 1964; Jaeger 1975; Jaeger & Schönlaub 1980, 1994; Corradini & Corriga 2012; Corradini *et al.* 2015, 2016). Our current knowledge of this area places the Carnic Alps as a distinct geographic region based on their unique features relative to other nearby Silurian peri-Gondwana sector areas, such as Bohemia (*e.g.* Ferretti & Kříž 1995, Štorch 2023 and references therein), Sardinia

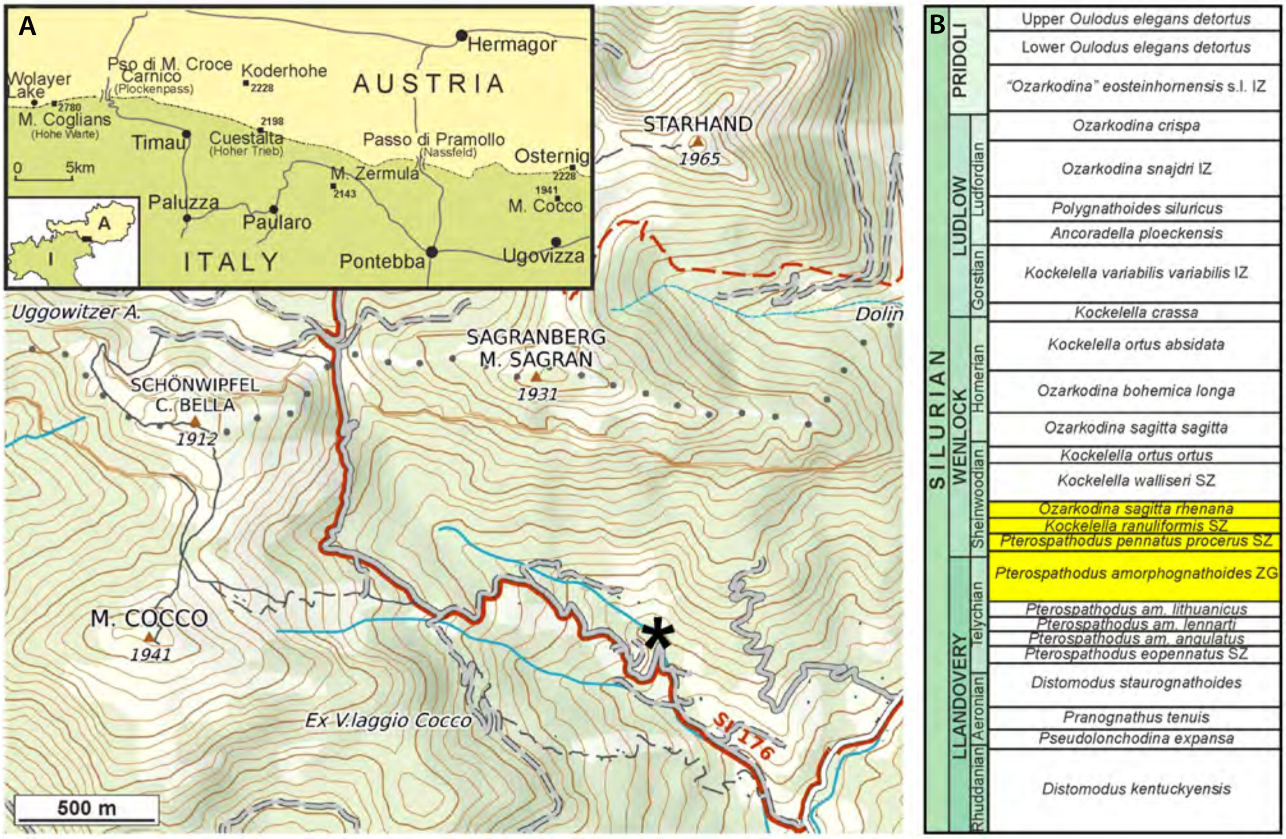

Figure 1. Location map of the area investigated in this study (A) and age assignment of the processed material (B). Silurian conodont zonation after Corradini *et al.* (2024).

(*e.g.* Barca *et al.* 1992; Corradini *et al.* 1998a, b, 2009; Ferretti *et al.* 1998; Ferretti & Serpagli 1999; Corradini & Ferretti 2009; Corriga *et al.* 2025), Spain (*e.g.* Gutiérrez-Marco *et al.* 1998, 2001), Montagne Noire (*e.g.* Feist & Schönlaub 1974, Štorch & Feist 2008) and Morocco (*e.g.* Corriga *et al.* 2014a, b), that are characterised by distinct common sequences and a less variable depositional setting.

The Silurian successions of the Carnic Alps, with a few significant sedimentary gaps at the base of the Silurian, at the Llandovery–Wenlock boundary and in the uppermost Wenlock Series (Schönlaub 1998, Corradini *et al*. 2015, Corriga *et al*. 2021), were formally subdivided into five formations (Corradini & Suttner 2015). Three calcareous units were deposited in the proximal parts of the basin: the Kok Formation (Telychian–lower Ludfordian), the Cardiola Formation (Ludfordian) and the Alticola Formation (upper Ludfordian–basal Lochkovian). Nautiloid cephalopods are abundant, associated with frequent trilobites, bivalves and conodonts as well as less common crinoids, gastropods, ostracods, brachiopods and chitinozoans (*e.g.* Brett *et al.* 2009, 2012; Corradini *et al.* 2010, 2015; Histon 2012). In the deeper part of the basin, the graptolitic black shales of the Bischofalm Formation were deposited in an anoxic environment. Transitional facies between calcareous and shaly facies is represented by the black graptolitic shales, marls and calcareous beds of the Nolbling Formation (Schönlaub 1997).

The Silurian strata cropping out in the eastern Carnic Alps (Fig. 1), north of Ugovizza, have been investigated geologically and economically for a long time. An intensive mining activity for iron and manganese is documented by mines active from as early as the 16th century to the first half of the 20th century (and possible cultivation since Roman times). Monte Cocco is an area where Silurian deposits are abundant and consist almost exclusively of cephalopod-rich limestones (Corradini *et al.* 2003). Outcrop conditions, however, are not optimal because of the abundant vegetation and the massive Quaternary cover. Only a few meters of limestones are discontinuously exposed, making it difficult to reconstruct a complete succession. The lower part of the Silurian, belonging to the Kok Formation, ranges from the Telychian (upper Llandovery) to the Gorstian (lower Ludlow), mostly represented by isolated blocks collected in the detritus near the mining galleries. These rocks are dark grey/black mudstones with millimetric marly intercalations. The upper part of the succession is represented by limestones characterised by a red coloration resulting from alteration and oxidation of abundant iron minerals, grading to light grey at the Silurian-Devonian boundary (Corradini *et al.* 2003, Corriga & Corradini 2009). The fossil content is rich and diversified, which has been reflected by intensive collecting activities by scholars and amateurs (Corradini *et al.* 2010). Nautiloid cephalopods (mostly Orthocerida) are undoubtedly the dominant fossils (*e.g.* Heritsch 1929; Gnoli & Histon 1998; Histon 1999; Gnoli *et al.* 2000; Serventi & Gnoli 2000; Serventi *et al*. 2000, 2007, 2010; Serventi 2001), associated with common bivalves (*e.g.* Kříž 1999, 2006), gastropods and trilobites. Crinoids, frequent as well, are documented only by disarticulated elements. Less common are brachiopods, often represented by small specimens, solitary rugose corals, machaeridians and a few conulariids (Corradini *et al.* 2010).

Material and methods

Study material. – This study is based upon a large set of conodont samples collected in the field as loose blocks along the Rio Tamer creek (sample code TAM BK), and treated in order to establish a precise biostratigraphic framework. Thirteen samples in particular, belonging to the Kok Formation, represent the bulk of the present work (Tab. 1). Conodont processing with the standard laboratory techniques (*i.e.* dissolution of carbonate rocks using dilute organic acids – acetic and formic – at concentrations ranging from 7 to 20% v/v, with the solution refreshed every 24 hours) by the use of formic acid was undertaken in the laboratories of the Department of Chemical and Geological Sciences (DSCG) of the University of Modena and Reggio Emilia (UNIMORE), Italy, and of the Department of Mathematics, Informatics and Geosciences of the University of Trieste, Italy. Eight uncovered polished thin sections (45 mm × 60 mm × 30 µm) were prepared from selected samples at the DSCG UNIMORE.

Table 1. List of samples investigated in the present study and their age assignment according to conodonts.

Unit	Sample	Conodont Zone	Age
KOK FORMATION	TAM BK-9	*Kockelella ranuliformis*	Homerian
	TAM BK-17	*Ozarkodina sagitta rhenana*	
	TAM BK-19	*Pt. pennatus procerus*	Homerian
	TAM BK-23		
	TAM BK-2	*Pt. amorphognathoides amorphognathoides*	Telychian–Homerian
	TAM BK-5		
	TAM BK-7		
	TAM BK-8		
	TAM BK-10		
	TAM BK-16		
	TAM BK-20		
	TAM BK-21		
	TAM BK-22		

Rock samples and prepared thin sections are housed in the "Inventario Paleontologia Università di Modena e Reggio Emilia (IPUM)" at the DSCG UNIMORE. Microfossils are stored in the collections of the Department of Mathematic, Informatic and Geosciences of Trieste University (DMGTS).

Analytical techniques. – Prepared materials were analysed by using optical, scanning electron, and environmental scanning electron microscopes (SEM, ESEM). Both electron microscopes were equipped with an Energy-Dispersive X-ray (EDX) detector for elemental microanalyses. Additionally, confocal Raman microscopy was used.

Individual ferruginous fossil replicas were picked from conodont residues using a Zeiss Stemi SV 11 binocular microscope (magnification 25–100×).

Thin sections were initially investigated by using a Jenapol transmitted and reflected optical light microscope, equipped with a Canon EOS 350D (at the DSCG UNIMORE).

Subsequently, carbon-coated selected specimens and thin-sections, mounted on aluminium stubs previously covered with carbon-conductive adhesive tape, were analysed (at the DSCG UNIMORE) using a JEOL JSM–6010PLUS/LA InTouchScope SEM. Measurements were performed in high vacuum with an accelerating voltage between 5 and 20 keV.

For X-ray powder diffraction analysis, representative batches of the extracted 3D coatings in samples TAM BK-8 and TAM BK-10 were hand-ground with an agate mortar and blended with 10 wt% corundum (α-Al_2O_2) NIST 676a as an internal standard. X-ray powder diffraction data were collected at the DSCG UNIMORE using a θ–θ Bragg-Brentano Panalytical X'Pert Pro Diffractometer with a Cu Kα radiation source ($\lambda = 1.5418$ Å) operating at 40 kV and 30 mA, equipped with a real-time multiple strip (RTMS) detector. Measurements were conducted over the 5–90° 2θ range with the following setup: 0.02 rad Soller slit, 10 mm mask, ¼° divergence slit, and ¼° anti-scatter slit on the incident beam; 5.0 mm anti-scatter slit and 0.02 rad Soller slit on the diffracted beam. The counting time was 160 seconds per 0.0167° 2θ step. Quantitative mineralogical analysis was conducted using the Rietveld method with the General Structure Analysis System (GSAS) software, employing EXPGUI as the graphical user interface. The analytical schemes and protocols followed those proposed by Gualtieri *et al.* (2019). Raw data were smoothed using low-pass filtering (convolution range = 5) before quantitative refinement, and the background was modelled with function 1 in GSAS, a Chebyshev polynomial of the first kind. Peak shapes were fitted using the Thompson–Cox–Hastings pseudo-Voigt function (function 2), while the March-Dollase function was applied as an intensity correction factor for preferred orientations. The initial structural models for refinement are provided in Table 2.

Raman spectroscopy was carried out at the University of Bologna, Italy, using a WITec Confocal Raman Microscope System alpha300R. Raman signals were acquired with a 100× Nikon objective (numerical aperture of 0.90, Nikon, Tokyo, Japan). The scans were performed using a frequency-doubled Nd-YAG laser (Newport, Evry, France) at an excitation wavelength of 532 nm, oriented perpendicular to the sample surface. To minimise laser-

Table 2. Quantitative mineralogical composition of samples TAM BK-8 and TAM BK-10. The standard deviation σQ (values in parenthesis) of the weight percentage Q for each phase was determined using the values from GSAS software output file after quantitative refinement, applying the formula $\sigma Q = \{[(\sigma a/a)^2 + (\sigma b/b)^2]^{1/2}\}\ Q$ (Young, 1962), where a and b are the two variables most affecting Q values and refer, respectively, to the weight fraction of the phase and the internal standard, whereas σa and σb are their standard deviations. Structural models for the refinement for birnessite, chamosite, goethite, hematite, quartz and siderite, are respectively from Blake *et al.* (1966), Effenberger *et al.* (1981), Kihara (1990), Hazemann *et al.* (1991), Walker & Bish (1992) and Lanson *et al.* (2002). χ2, *Rp*, and *Rwp*. are statistical tools primarily used to assess the goodness-of-fit or independence between observed mineralogical data and expected distributions or relationships; see Gualtieri *et al.* (2019) and reference therein for further details.

	Chemical formula	MC BK-8 (wt%)	MC BK-10 (wt%)
Birnessite	$(Na,Ca,K)x(Mn^{4+},Mn^{3+})_2O_4\cdot 1.5(H_2O)$	1.5(1)	1.44(9)
Chamosite	$(Fe^{2+}{}_3Mg_{1.5}AlFe^{3+}{}_{0.5}Si3AlO_{12}(OH)_6)$	6.7(4)	8.2(4)
Goethite	(α-$Fe^{3+}O(OH)$	33.6(4)	28.8(4)
Hematite	(α-Fe_2O_3)	3.6(3)	13.9(3)
Quartz	SiO_2	8.0(1)	4.90(9)
Siderite	$FeCO_3$	3.7(1)	4.7(2)
Amorphous		43.0(7)	38.1(7)
χ^2		0.9803	0.9021
R_p (%)		0.0170	0.0162
R_{wp} (%)		0.0217	0.0203

induced thermal effects, the laser excitation intensity was carefully adjusted at the sample surface, ensuring an optimal signal-to-noise ratio. Two-dimensional (x-y) Raman maps were acquired, and data processing was performed using the WITec Project Management and Image Project Plus software suite.

Results

Remarks on faunistic content. – Representatives of benthos constitute the major part of the preserved faunal assemblage documented by the Tamer residues. In order of abundance, we were able to identify bivalves, trilobites,

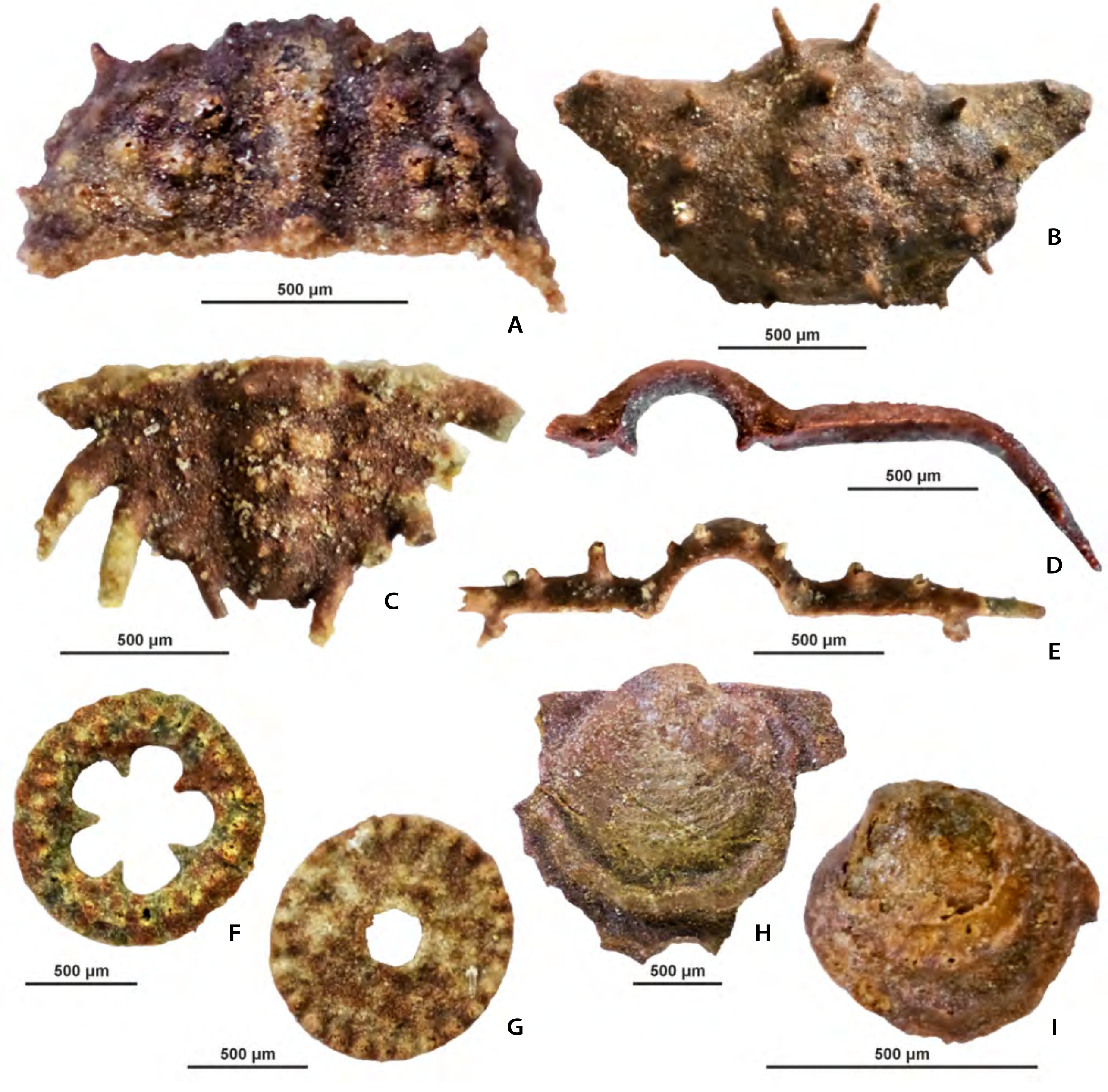

Figure 2. Photographic images of selected material recovered in the conodont residues of the Kok Formation, Tamer area, Italy. Note the reddish-greenish colour of the specimens. • A–E – ferruginous coatings around trilobite skeletal elements. A, B – upper views of cephalons DMGTS 116 and DMGTS 117, sample TAM BK-22, *Pterospathodus amorphognathoides amorphognathoides* Zone. C – upper view of pygidium DMGTS 118, sample TAMER BK-22, *Pterospathodus amorphognathoides amorphognathoides* Zone. D, E – lateral views of thoracic segments DMGTS 119 and DMGTS 120, sample TAMER BK-22, *Pterospathodus amorphognathoides amorphognathoides* Zone. • F, G – echinoderm skeletal elements. Upper views of DMGTS 121 and DMGTS 122, sample TAM BK-22, *Pterospathodus amorphognathoides amorphognathoides* Zone. • H, I – internal moulds of bivalve skeletal elements. H – upper view of DMGTS 123, sample TAM BK-19, *Pterospathodus pennatus procerus* Zone. I – upper view of DMGTS 124, sample TAM BK-22, *Pterospathodus amorphognathoides amorphognathoides* Zone.

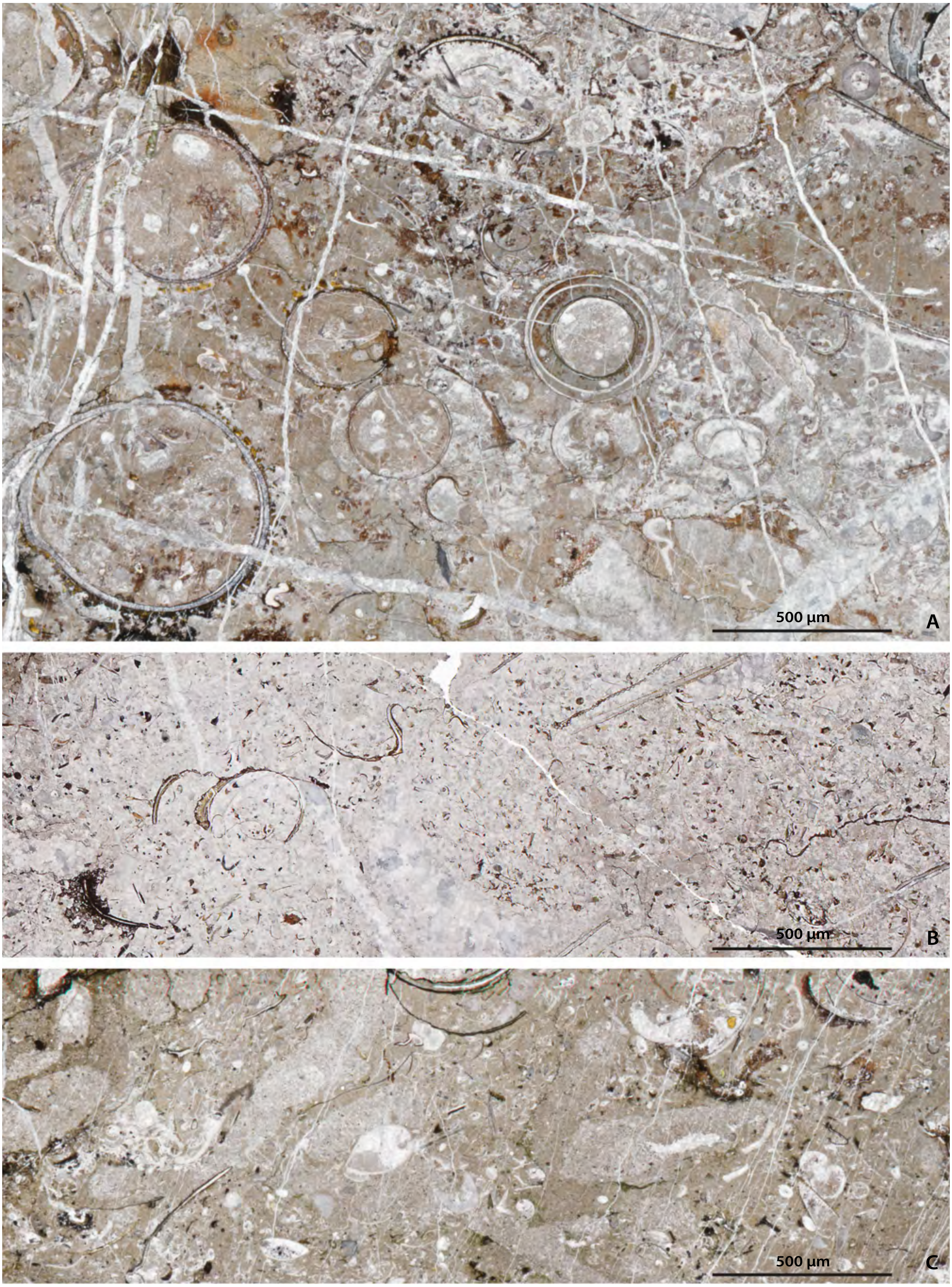
500 µm
A
500 µm
B
500 µm
C

ostracods, crinoids, gastropods, brachiopods, foraminifers and sparse remains of other invertebrate groups (Fig. 2). Very few nautiloids have been recovered. Bivalves (Fig. 2H, I), gastropods and ostracods are almost exclusively preserved as internal moulds, aside from a few external coatings. Crinoids (Fig. 2F, G) are represented by rare calices and holdfasts, and abundant and diverse stem fragments mostly preserved by external coatings. Trilobites (Fig. 2A–E) were recovered as fragmentary remains with numerous cephalons and pygidia, as well as isolated thoracic segments. The outer surface of the specimens recovered from conodont residues appears granular and patchy. The material exhibits a reddish-brown to orange colour (Fig. 2A–C) with areas grading to green (Fig. 2F). A rich conodont fauna enabled a precise age assignment. The association documents a shallow and well-oxygenated environment dominated by shelly faunas.

In thin sections, light-grey to reddish-pink wackepackstones with abundant cephalopod and trilobite remains (Fig. 3) offer a more realistic picture of the fauna that was present at that time (conodont residues illustrate only what survived acid leaching). The skeletal elements expose laminated ferruginous constructions developed either on the outer and/or the inner surface of the shell (Fig. 3A). Trilobites and cephalopods appear to be the most frequently coated skeletal elements. These laminated coatings can be partial, comprising multiple layers that grow over specific areas of the shell, or they may completely envelop the organism. Laminae reveal arborescent to dendrolitic morphologies. Typically, the coatings begin to form on prominent parts of the shell or at its extremities, forming isolated or multiple domes. The internal structure of these domes discloses alternating layers: white sparry laminae, interspersed with darker laminae ranging in colour from yellow to green to red. The laminae vary in continuity, with some being more uniform than others. Equidimensional biodebris is scattered within a finer matrix of articulated and disarticulated bivalves, ostracods, gastropods, and echinoderm ossicles, associated with abundant trilobite and cephalopod fragments (Fig. 3B, C).

Mineralogical analyses. – XRPD analyses were run on 3D ferruginous coatings extracted from conodont residues. From a strictly qualitative point of view, results show the presence of six mineralogical phases, *i.e.* goethite, chlorite, siderite, hematite, quartz, and birnessite (a naturally occurring hydrous manganese dioxide possibly containing other cations), along with a significant amount of amorphous material. Table 2 illustrates the quantitative phase analyses results. Mineralogical data are in good agreement with SEM-EDS measurements performed on the same 3D material (Fig. 5). Regarding the chlorite-group minerals, the best fit in the mineralogical analysis was obtained using the chamosite structure, a greenish, iron-rich chlorite occasionally occurring in

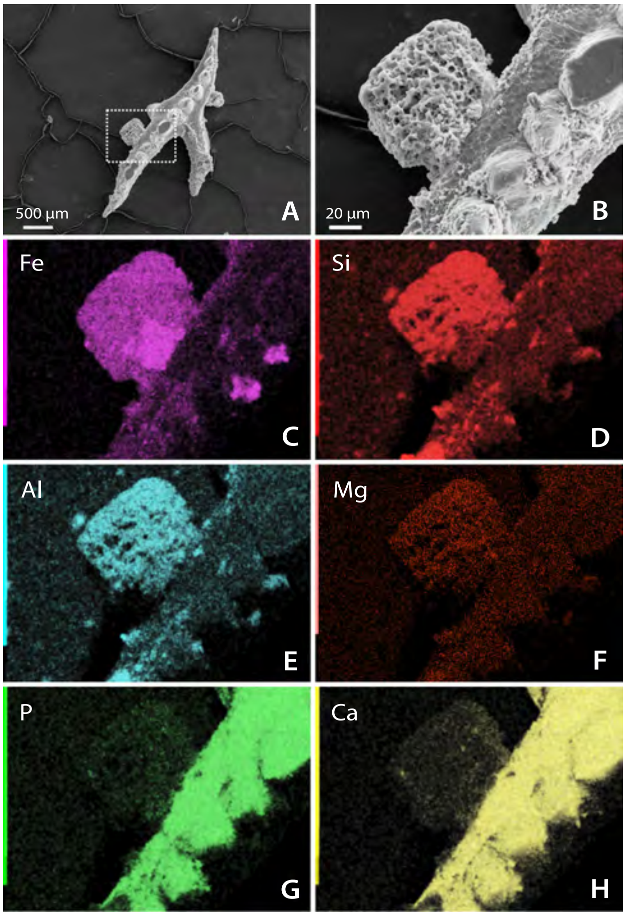

Figure 4. Secondary electron (SE) images and energy dispersive X-ray spectroscopic (EDS) elemental maps of a ferruginous overgrowth around a conodont element. • A, B – SE image of the conodont *Pterospathodus pennatus procerus* with a crust laterally overgrown on a process (the inset in A is detailed in B); sample TAM BK-23, *Pterospathodus pennatus procerus* Zone. • C–H – Fe, Si, Al, Mg, P and Ca maps of B. Colour intensity corresponds to relative elemental abundance. Note the joined increase of Fe, Si, Al and Mg in the crust overgrown on the conodont element (dominated by P and Ca enrichments).

< Figure 3. Transmitted-light micrographs of petrographic thin-sections illustrating main microfacies of the Kok Formation exposed in the Tamer area. • A – cephalopod packstone with abundant ferruginous coatings around skeletal elements. Note the frequent telescoping of cephalopod shells. Sample TAM BK-2, Kok Formation, Pterospathodus amorphognathoides amorphognathoides Zone. • B, C – scattered fine ferruginous biodebris (mostly trilobite elements) giving a reddish colour to the matrix. Note well-developed coating around a skeletal element on the left bottom in (A) and (B). Samples TAM BK-8 and TAM BK-10, Kok Formation, Pt. amorphognathoides amorphognathoides Zone.

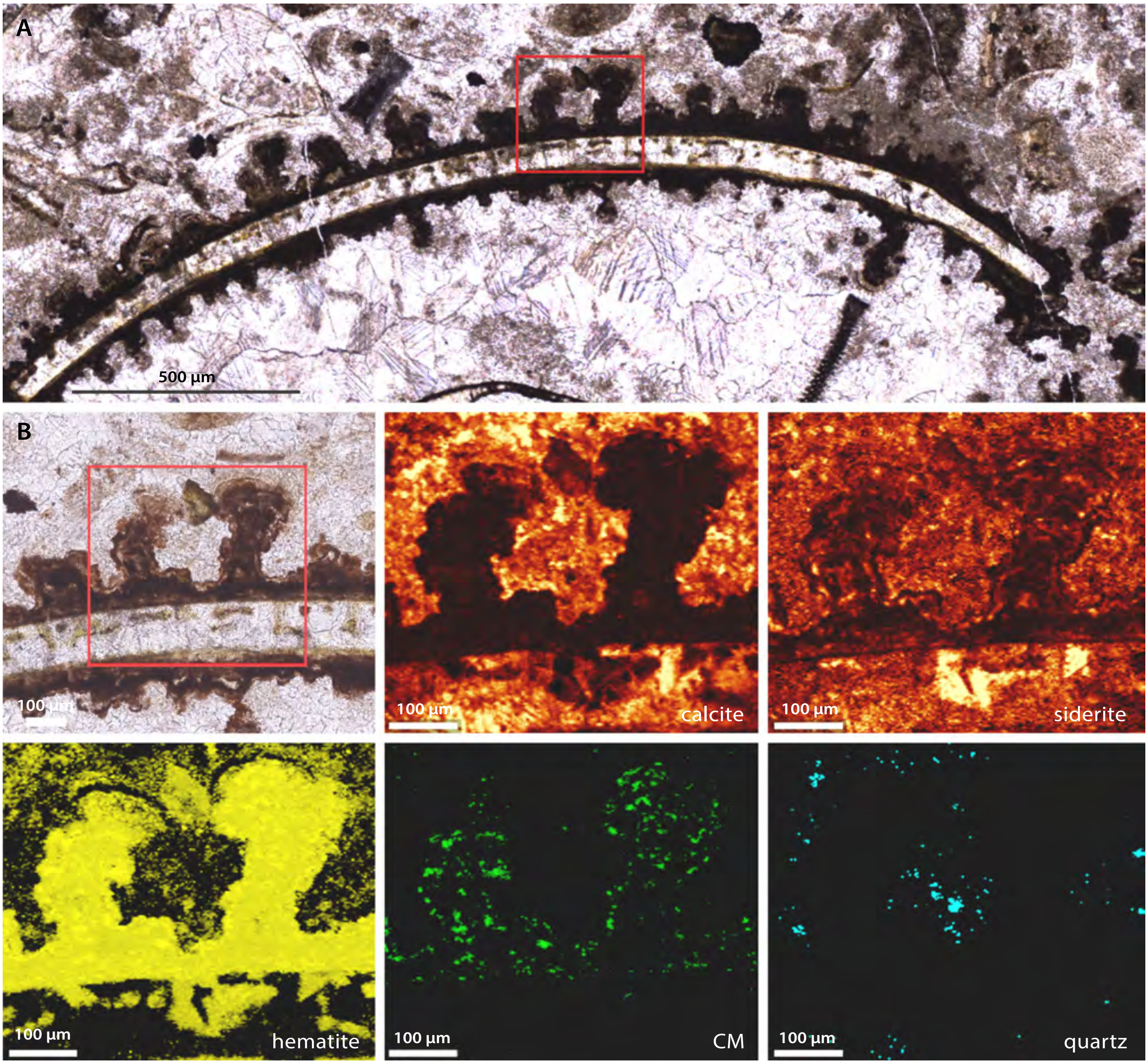

Figure 5. A – transmitted light optical photomicrograph of a petrographic thin section (sample TAM BK-2) showing a ferruginous multi-columnar laminated coating around both sides of a cephalopod shell. The boxed area is magnified in the following photo. • B – details of the microstromatolitic structures. Following panels are Raman maps obtained within the area included in the red square (in B) and represent calcite as seen from the intensity of the 1085 cm^{-1} diagnostic peak, siderite as seen from the intensity of the 1091cm^{-1} diagnostic peak, hematite as seen from the intensity of the 1313 cm^{-1} diagnostic peak, carbonaceous material (CM) as seen from the intensity of the ~1345 D and ~1600 cm^{-1}G diagnostic peaks, and quartz as seen from the intensity of the 464 cm^{-1} diagnostic peak (see also Fig. 6).

low- to medium-grade metamorphic rocks and iron-rich sedimentary rocks, especially ironstones and marine shales (Tang *et al.* 2017, Luan *et al.* 2024).

The global composition is consistent with the abundant occurrence of the ferriferous minerals mentioned above and with previous literature related to coeval or even older material from nearby areas in the Carnic Alps. Ferretti (2005), Ferretti *et al.* (2012) and Corriga *et al.* (2021), by the application of the same analytical protocol, described similar ferruginous laminated coatings around skeletal fragments (mostly trilobites and some cephalopods and echinoderms) with a distinct stromatolitic pattern in pink to red limestones of Silurian age. The laminated structure exhibited rhythmic alternations of goethite, hematite, magnetite, and chamosite with intercalated calcite layers. The co-occurring presence of carbonaceous matter and fossilised microbial structures reinforced a microbial role in explaining their genesis (Ferretti *et al.* 2012). Ferruginous coatings surrounding skeletal fragments in the Upper Ordovician strata of the Cellon section have

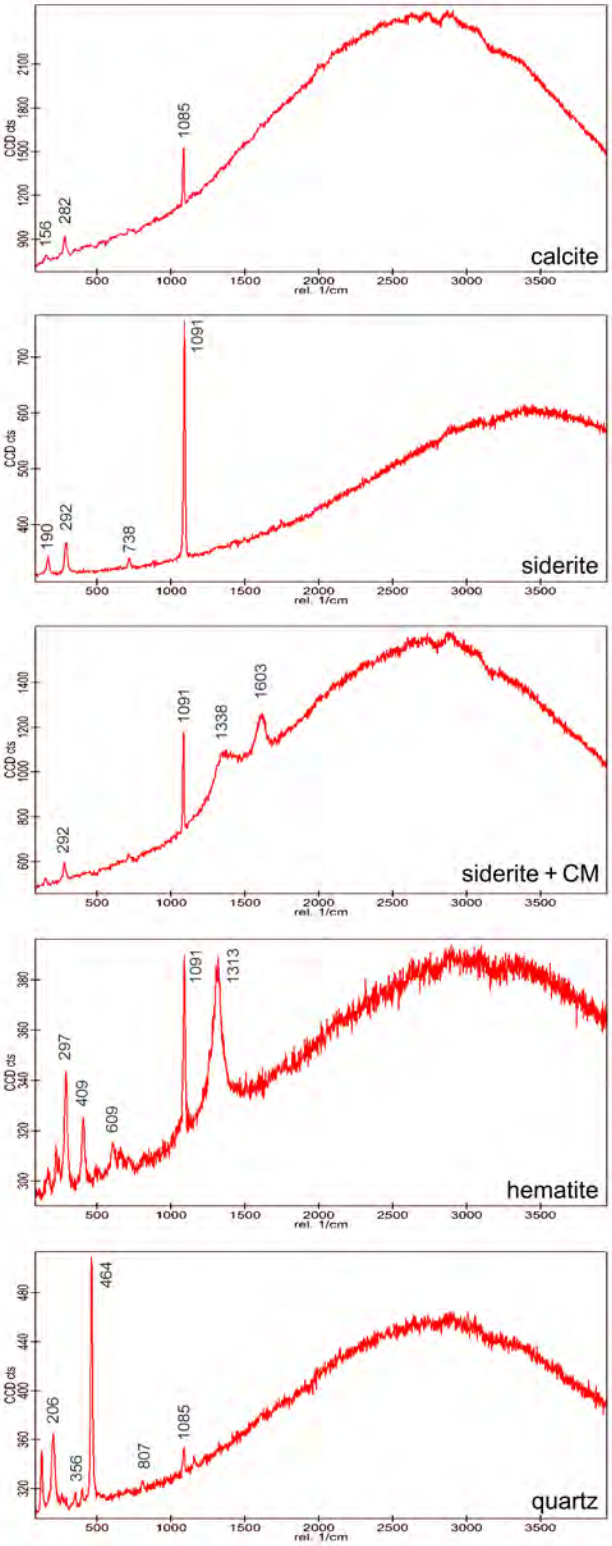

Figure 6. Representative Raman spectra of the mineral phases observed in the calcite (Raman bands: 156, 282, 1085 cm^{-1}), siderite (Raman bands: 190, 292, 738, 1091 cm^{-1}), carbonaceous material, CM (Raman bands: 1338 cm^{-1}, D; 1603 cm^{-1}, G), hematite (Raman bands: 297, 409, 609, 1313 cm^{-1}), quartz (Raman bands: 206, 356, 464, 807 cm^{-1}), maps shown in Figure 5 (Cavalazzi *et al.* 2012, Frezzotti *et al.* 2012).

recently revealed the earliest known laminated structures in the Carnic Alps, characterised by red to greenish layers composed of alternating chamosite and goethite, interbedded with calcite bands (Ferretti *et al.* 2023a). As for the Tamer material (see below), Raman analysis run on the coatings did not reveal the presence of goethite, clearly indicated by X-ray investigation. However, the Raman analytical conditions applied in the study could have possibly transformed goethite into hematite (Foucher 2021).

As will be later discussed, this assemblage reflects a complex interplay of sedimentary, diagenetic, and mild post-depositional processes that shaped the mineralogical signature of the Rio Tamer samples.

Raman spectroscopy. – Raman mapping was run on thin sections specifically prepared to expose the multi-layered structure of the 3D coatings around skeletal elements. The ferruginous laminae, surrounding cephalopod shells with inner and outer coatings in Figure 5, reveal the ubiquitous presence of hematite, with subordinate siderite, embedded within a mineral matrix primarily composed of calcite and quartz grains. Additionally, the detection of carbonaceous matter (CM) within the laminae was confirmed by the intensity of the diagnostic D (~ 1345 cm^{-1}) and G (~ 1600 cm^{-1}) peaks in the Raman spectra (Fig. 6), indicating the presence of organic residues.

Discussion

Iron minerals and ironstones are anything but rare in fossil preservation, as documented by a full range of reports throughout the Phanerozoic or even before (*e.g.* Rudmin *et al.* 2020, 2022; Matheson *et al.* 2022 and references therein; Papazzoni *et al.* 2022), and still active today (*e.g.* Di Bella *et al.* 2019, 2021). Despite thorough research, a consensus has yet to emerge on the dynamics ruling the genesis of these occurrences.

A special case is represented by ferruginous skeletal replicas, which occur only infrequently. External moulds and casts preserved in iron documented the soft-bodied late Proterozoic Ediacaran benthic organisms referred to as "Vendobionta", populating substrates between fair-weather and storm wave-base. Gehling (1999) proposed that a sort of "death mask" resulting from bacterial precipitation of iron minerals was able to explain the retention of an external mould of the soft-bodied organism in the sediment and, at the same time, the replacement of the decaying body with the formation of a cast.

A similar preservational pathway *via* biologically precipitated biofilms made of aluminosilicate phases on fossil leaves was suggested by Locatelli *et al.* (2017). The authors introduced a specific "Biofilm-Clay Template"

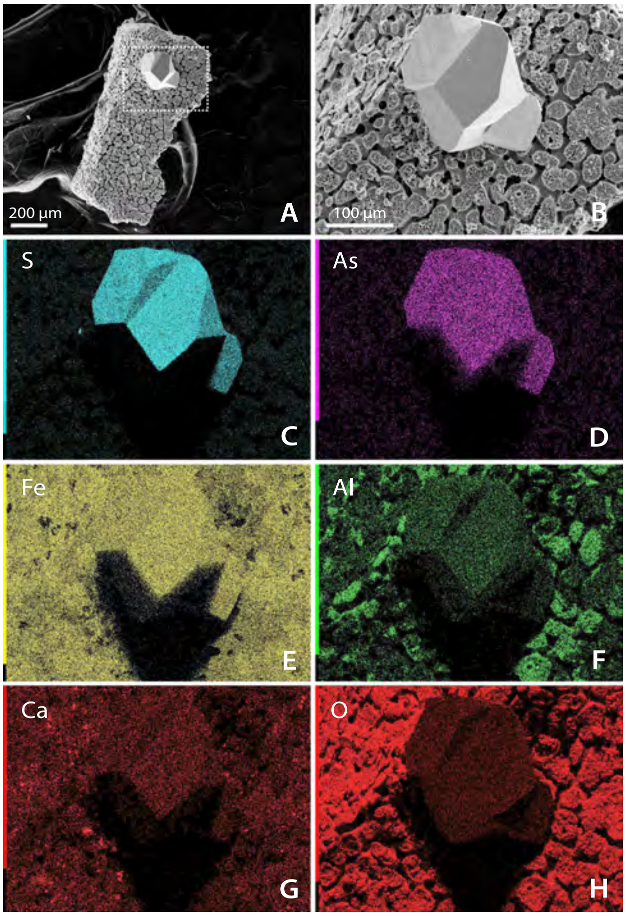

Figure 7. Secondary electron (SE) images and energy dispersive X-ray spectroscopic (EDS) elemental maps of a peculiar echinoderm ossicle with a crystal overgrown on it. • A, B – SE image of the echinoderm skeletal element (the inset in A is detailed in B); sample TAM BK-23, *Pterospathodus pennatus procerus* Zone. • C–H – S, As, Fe, Al, Ca and O maps of B. Colour intensity corresponds to relative elemental abundance. Note the joined increase of S and As in the crystal.

taphonomic model of microbially mediated clay authigenesis. Spicer (1977) had articulated an analogous microbial mineralization process, experimentally reporting the presence of a thin layer of iron oxides with small amounts of aluminosilicates on modern leaves within weeks of submersion in a freshwater stream and delta. That layer was strictly comparable with the iron enrichment observed on the surface of Cretaceous leaves. Locatelli *et al.* (2017) successfully expanded the tests of Spicer (1977) and Dunn *et al.* (1997) to fossil and recent leaves spanning in age from the Cretaceous to the Oligocene and documenting different settings. According to their results, a biofilm forms after the leaf enters the depositional environment, though the extent of this process largely depends on the specific environmental conditions (*i.e.* subaerially, oxygenated, dysoxic, or anoxic water or sediments). Dissolved metals in the form of either free ions or oxides/oxyhydroxides (predominantly aluminium and iron species) adsorb to the biofilm, providing binding sites for silica, and, ion availability permitting, triggering the nucleation of nanocrystalline, poorly ordered aluminosilicates and their precursors on the surface and within the biofilm, thus forming a biofilm-clay template. This template may later endorse different fossilization pathways depending on the depositional setting (oxygenation, *etc.*) and original composition of the biofilm-clay template.

Retallack (2022) applied the "death-mask" model to the Ediacaran biota, proposing that ferruginous biofilms are triggered not by sulphate-reducing bacteria as suggested by Gehling (1999) but by filamentous, iron-oxidizing bacteria provided with adhesive bases able to form robust biofilms. These biofilms commonly transform to hematite during burial starting from iron oxyhydrates precipitated by aerobic iron-oxidizing bacteria that consume organic matter of the organism tissue shortly after death. Clayey oxidised biofilms have been reported from lakes and soils; however crystalline chlorite films have likewise been reported on marine fossil compressions (*e.g.* Gámez Vintaned *et al.* 2011, Wan *et al.* 2020, Becker-Kerber *et al.* 2022).

All studies reported above indicate that ferruginous biofilms are frequently involved in fossilization processes of soft-bodied organisms. The effectiveness of this mechanism is further amplified when it targets skeletal elements that are already predisposed to mineralization, a process facilitated by the intrinsic presence of hard anatomical structures. These pre-existing rigid components not only provide a favourable microenvironment for mineral deposition but also act as nucleation sites that enhance the stability and growth of mineral phases, thereby promoting more efficient biomineralization. An environment rich in iron sources like the Carnic Alps served as an ideal geochemical setting to support the action of biomineralising microbial communities. A benthic assemblage comprising trilobites, bivalves, brachiopods, gastropods, and echinoderms, associated with redeposited cephalopod conchs, contributed a substantial quantity of calcareous skeletal material which likely provided optimal substrates for the nucleation and development of iron-rich biofilms (Fig. 8A). The formation of the laminated pattern observed in the iron coatings appears to have resulted from the repeated activation of the process. This iterative mechanism likely reflects fluctuating environmental conditions or biological activity that governed the episodic accumulation of iron-rich layers over time. Depending on the oxygenation levels, both Fe^{2+} and Fe^{3+} may have been available at diverse times and/or contemporaneously, and rule out the different iron phases documented by the coatings/moulds (Fig. 8B).

Overall, the mineralogical associations in the Rio Tamer samples can be interpreted largely through the lens of early diagenetic transformations under diverse redox

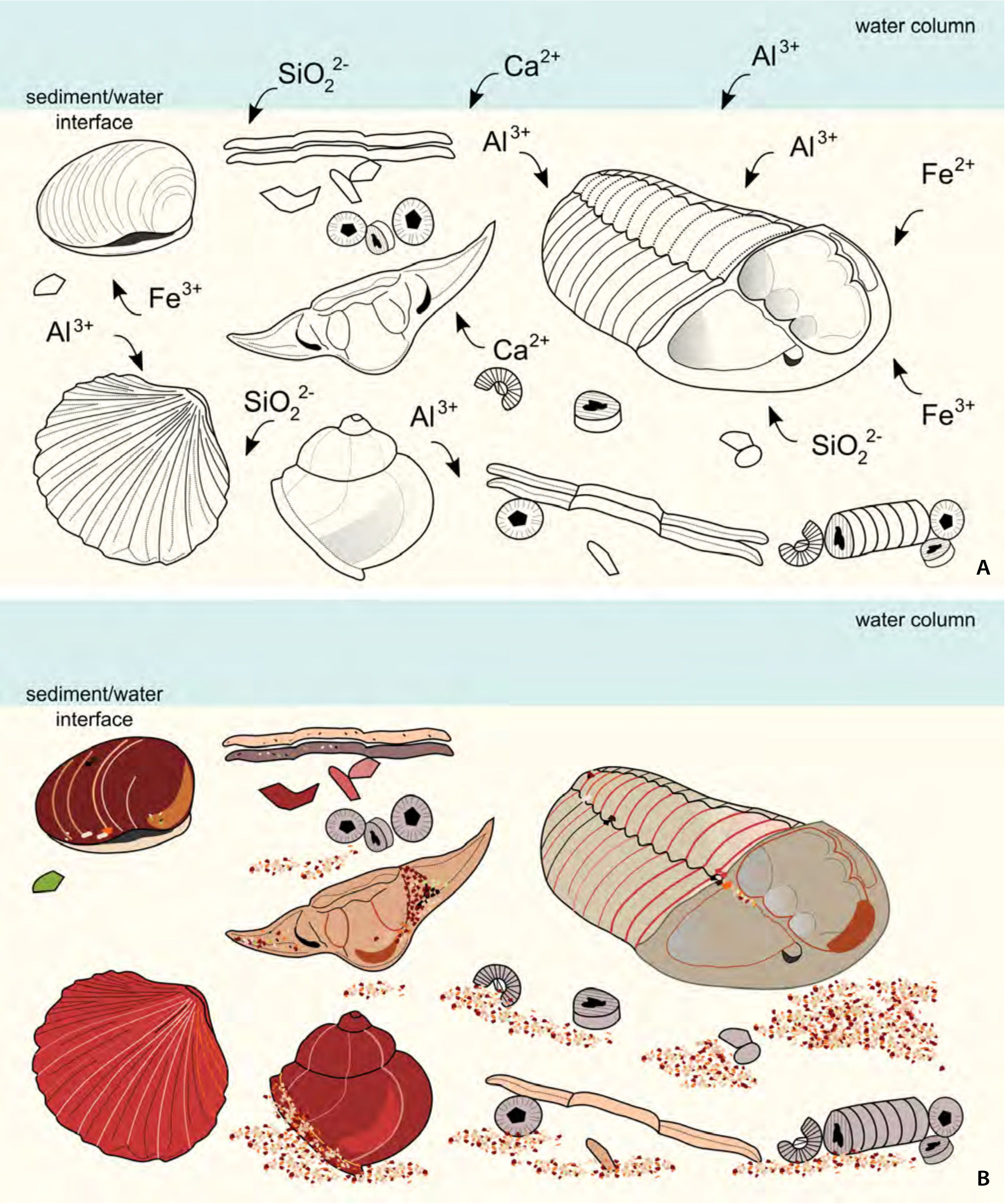

Figure 8. Proposed taphonomic scenario of the Carnic material investigated in this study following the Biofilm-Clay Template model of Locatelli *et al*. (2017) for Vendobionta. • A – depositional environment where benthic communities (here represented by brachiopods, bivalves, trilobite skeletal elements and echinoderm ossicles) are locally colonised by microbial mats which form a biofilm. Metal and silicon ions in solution adhere to the biofilm, leading to the formation of clay mineral precursors as microbial decomposition continues. Oxygen availability strongly varies depending on whether the skeletal element is in contact with the water column or enclosed in sediments. • B – continued clay minerals precipitation within the biofilm results in fossil coatings and moulds of various chemical compositions, indicated by the diverse reddish colours of the ferruginous bioclasts, which, in turn, indicate the different iron oxides and hydroxides replicating the original organisms.

regimes, coupled with the availability of Fe, Mn, and minor carbonate alkalinity within a dynamic depositional setting (Canfield 2005, Raiswell & Canfield 2012). The abundance of iron oxides and hydroxides (hematite and goethite) points to an intense oxidation, possibly related to exposure to oxygenated fluids. Chamosite, on the opposite, provides evidence for an anoxic/reducing depositional environment. This layer silicate typically forms in marine sedimentary settings under reducing conditions, frequently in association with iron-rich deposits or as a diagenetic product of pre-existing clay minerals (Tang *et al.* 2017, Luan *et al.* 2024). A similar consideration applies to siderite; however, its crystallisation requires less reducing conditions and a weakly alkaline pore water, where iron is available as Fe^{2+} and carbonate alkalinity is sufficient to drive precipitation (Mozley & Wersin 1992, Mücke 2006). Although in some geological contexts these minerals are linked to low-temperature hydrothermal systems, their development can equally occur through reaction of detrital clay precursors with Fe^{2+} in pore fluids under modest burial temperatures (Hillier 1994, Worden *et al.* 2020). A hydrothermal activity may be suggested as well by the occurrence, albeit modest, of birnessite. Indeed, birnessite can form in Mn-rich rocks altered by weathering or hydrothermal activity. This occurs under conditions of fluctuating redox potentials, typically at (or near) the sediment-water interface where minor oxidative pulses promote Mn^{2+} oxidation, especially in pore waters, where these fluctuating conditions cause repeated cycles of oxidation and precipitation (Post 1999, Tebo *et al.* 2004, Feng *et al.* 2008, Papadopoulos *et al.* 2019, Baudet *et al.* 2024). Like birnessite, also the occurrence of Fe, As and S possibly forming arsenopyrite crystals (Fig. 7C–E) not detectable through XRPD as in reduced quantity, is not sufficient to definitively confirm the hydrothermal imprint, as diagenetic sulphides within carbonaceous sediments can form during early diagenesis in anoxic environments (Rddad 2017, Armstrong *et al.* 2019).

The diagenetic overprint is confirmed also by quartz, which, in limestones, could result from crystallisation of silica of detrital or hydrothermal origin. Similarly, the amorphous material detected may include poorly ordered clays, silica gels, or fine-grained Fe-Mn oxyhydroxides, products typical of early diagenetic reactions under variable pH and Eh conditions (Berner 1980).

Conclusion

Conodont residues from the Silurian Kok Formation in the Tamer area (Carnic Alps, Italy) have yielded three-dimensional ferruginous coatings and moulds of originally calcareous organisms, primarily belonging to benthic faunas. Bivalves, gastropods, nautiloids, brachiopods, trilobites, ostracods, crinoids, foraminifers, and other minor components, all preserved in various iron phases (*e.g.* goethite, hematite, chamosite and siderite), often co-occurring within the same specimen. While a modest hydrothermal influence cannot be entirely excluded, particularly in enhancing local metal mobility, the mineral suite aligns well with typical diagenetic sequences in iron-rich sedimentary systems.

A microbial involvement in the growth of the skeletal replicas is evidenced by the presence of carbonaceous matter within the ferruginous coatings. We propose that microbial activity facilitated a unique preservation pathway, leveraging available iron sources in a shallow, ferruginous marine system to enable fossilisation under conditions typically unfavourable for preservation of calcareous organisms.

Acknowledgements

Our sincere thanks to Carl Brett and to an anonymous reviewer for constructive criticism and valuable comments that significantly improved the quality of the manuscript. This research was undertaken within the framework and with the financial support of the European Community – Next Generation EU, Italian Ministry of University and Research, Project P2022K9BE8, PRIN-PNRR 2022 "OCEANS" (AF), Project 2022MAM9ZB, PRIN-2022 "BIOVERTICES" (AF) and Project 2022ZH5RWP, PRIN-2022 "DEEP PAST" (CC). This study is a contribution to Space It Up project funded by the Italian Space Agency, ASI, and the Ministry of University and Research, MUR (n. 2024-5-E.0 - CUP n. I53D24000060005) (BC). This paper contributes to the IGCP Project n. 652 "Reading geologic time in Palaeozoic sedimentary rocks".

References

Armstrong, J.G.T., Parnell, J., Bullock, L.A., Boyce, A.J., Perez, M. & Feldmann, J. 2019. Mobilisation of arsenic, selenium and uranium from Carboniferous black shales in west Ireland. *Applied Geochemistry 109*, 104401. DOI 10.1016/j.apgeochem.2019.104401

Barca, S., Ferretti, A., Massa, P. & Serpagli, E. 1992. The Hercynian Arburese tectonic unit of SW Sardinia new stratigraphic and structural data. *Rivista Italiana di Paleontologia e Stratigrafia 98*, 119–136.

Baudet, C., Bucciarelli, E., Sarthou, G., Boulart, C., Pelleter, E., Goddard-Dwyer, M., Whitby, H., Zhang, R., Obernosterer, I., González-Santana, D., Léon, M., van Beek, P., Sanial, V., Jeandel, C., Vivier, F., Vorrath, M.-E., Liao, W.-H., Germain, Y. & Planquette, E. 2024. A hydrothermal plume on the Southwest Indian Ridge revealed by a multi-proxy approach: Impact on iron and manganese distributions (GEOTRACES GS02). *Marine Chemistry 265–266*, 10401. DOI 10.1016/j.marchem.2024.104401

Becker-Kerber, B., Abd Elmola, A., Zhuravlev, A., Gaucher, C., Simões, M.G., Prado, G.M.E.M., Gámez Vintaned, J.A., Fontaine, C., Lino, L.M., Ferreira Sanchez, D., Galante, D., Paim, P.S.G., Callefo, F., Kerber, G., Meunier, A. & El Albani, A. 2022. Clay templates in Ediacaran vendotaeniaceans: Implications for the taphonomy of carbonaceous fossils. *GSA Bulletin 134*, 1334–1346. DOI 10.1130/B36033.1

Berner, R.A. 1980. *Early Diagenesis: A Theoretical Approach*. 256 pp. Princeton University Press, Princeton. DOI 10.1515/9780691209401

Blake, R.L., Hessevick, R.E., Zoltai, T. & Finger, L.W. 1966. Refinement of the hematite structure. *American Mineralogist 51*, 123–129.

Brett, C.E., Ferretti, A., Histon, K. & Schönlaub, H.P. 2009. Silurian sequence stratigraphy of the Carnic Alps, Austria. *Palaeogeography, Palaeoclimatology, Palaeoecology 279,* 1–28. DOI 10.1016/j.palaeo.2009.04.004

Brett, C.E., McLaughlin, P.I., Histon, K., Schindler, E. & Ferretti, A. 2012. Time specific aspects of facies: state of the art, examples, and possible causes. *Palaeogeography, Palaeoclimatology, Palaeoecology 367–368*, 6–18. DOI 10.1016/j.palaeo.2012.10.009

Briggs, D.E.G. 2003. The role of decay and mineralization in the preservation of soft-bodied fossils. *Annual Review of Earth and Planetary Sciences 31*, 275–301. DOI 10.1146/annurev.earth.31.100901.144746

Canfield, D.E. 2005. The early history of atmospheric oxygen: Homage to Robert M. Garrels. *Annual Review of Earth and Planetary Sciences 33*, 1–36. DOI 10.1146/annurev.earth.33.092203.122711

Cavalazzi, B., Barbieri, R., Cady, S.L., George, A.D., Gennaro, S., Lui, A., Westall, F., Rossi, A.P., Ori, G.G. & Taj-Heddine, K. 2012. Iron-framboids in the hydrocarbon-related Middle Devonian Hollard Mound of the Anti-Atlas mountain range in Morocco: evidence of potential microbial biosignatures. *Sedimentary Geology 263–264*, 183–193. DOI 10.1016/j.sedgeo.2011.09.007

Corradini, C. & Corriga, M.G. 2012. A Pridoli-Lochkovian conodont zonation in Sardinia and the Carnic Alps: implications for a global zonation scheme. *Bulletin of Geosciences 87*, 635–650. DOI 10.3140/bull.geosci.1304

Corradini, C. & Ferretti, A. 2009. The Silurian of the External Nappes (southeastern Sardinia). *Rendiconti della Società Paleontologica Italiana 3*, 43–49.

Corradini, C. & Suttner, T. (eds) 2015. The Pre-Variscan sequence of the Carnic Alps (Austria and Italy). *Abhandlungen der Geologischen Bundesanstalt 69*, 1–158.

Corradini, C., Ferretti, A. & Serpagli, E. 1998a. The Silurian and Devonian sequence in SE Sardinia. *Giornale di Geologia 60*, 71–74.

Corradini, C., Ferretti, A., Serpagli, E. & Barca, S. 1998b. The Ludlow-Pridoli Section "Genna Ciuerciu" west of Silius. *Giornale di Geologia 60*, 112–118.

Corradini, C., Pondrelli, M., Serventi, P. & Simonetto, L. 2003. The Silurian cephalopod limestone in the Mt. Cocco area (Carnic Alps, Italy): Conodont biostratigraphy. *Revista Española de Micropaleontología 35*, 285–294.

Corradini, C., Corriga, M.G., Ferretti, A. & Leone, F. 2009. The Silurian of the Foreland Zone (southwestern Sardinia). *Rendiconti della Società Paleontologica Italiana 3,* 51–56.

Corradini, C., Corriga, M.G., Pondrelli, M., Serventi, P. & Simonetto, L. 2010. Il Siluriano di Monte Cocco (Alpi Carniche). *Gortania Geologia, Paleontologia, Paletnologia 31*, 23–30.

Corradini, C., Corriga, M.G., Männik, P. & Schönlaub, H.P. 2015. Revised conodont stratigraphy of the Cellon section (Silurian, Carnic Alps). *Lethaia 48*, 56–71. DOI 10.1111/let.12087

Corradini, C., Pondrelli, M., Simonetto, L., Corriga, M.G., Spalletta, C., Suttner, T.J., Kido, E., Mossoni, A. & Serventi, P. 2016. Stratigraphy of the La Valute area (Mt. Zermula massif, Carnic Alps, Italy). *Bollettino della Società Paleontologica Italiana 55*, 55–78. DOI 10.4435/BSPI.2016.06

Corradini, C., Henderson, C., Barrick, J.E. & Ferretti, A. 2024. Conodonts in Biostratigraphy. A 300-million-years long journey through geologic time. *Newsletters on Stratigraphy*, prepublication paper 2024, 1–40. DOI 10.1127/nos/2024/0822

Corriga, M.G. & Corradini, C. 2009. Upper Silurian and Lower Devonian conodonts from the Monte Cocco II Section (Carnic Alps, Italy). *Bulletin of Geosciences 84*, 155–168. DOI 10.3140/bull.geosci.1112

Corriga, M.G., Corradini, C. & Walliser, O.H. 2014a. Upper Silurian and Lower Devonian conodonts from Tafilalt, southeastern Morocco. *Bulletin of Geosciences 89*, 183–200. DOI 10.3140/bull.geosci.1473

Corriga, M.G., Corradini, C., Haude, R. & Walliser, O.H. 2014b. Conodont and crinoid stratigraphy of the upper Silurian and Lower Devonian scyphocrinoid beds of Tafilalt, southeastern Morocco. *GFF 136*, 65–69. DOI 10.1080/11035897.2013.862849

Corriga, M.G., Corradini, C., Pondrelli, M., Schönlaub, H.-P., Nozzi, L., Todesco, R. & Ferretti, A. 2021. Uppermost Ordovician to lowermost Devonian conodonts from the Valentintörl section and comments on the post Hirnantian hiatus in the Carnic Alps. *Newsletters on Stratigraphy 54,* 183–207. DOI 10.1127/nos/2020/0614

Corriga, M.G., Ferretti, A. & Corradini, C. 2025. Upper Silurian conodonts from the Ockerkalk limestone of southeastern Sardinia (Italy). *Bulletin of Geosciences 100(4),* 445–487. DOI 10.3140/bull.geosci.1930

Di Bella, M., Sabatino, G., Quartieri, S., Ferretti, A., Cavalazzi, B., Barbieri, R., Foucher, F., Messori, F. & Italiano, F. 2019. Modern iron ooids of hydrothermal origin as a proxy for ancient deposits. *Scientific Reports 9*, 1–9. DOI 10.1038/s41598-019-43181-y

DiBella, M., Pirajno, F., Sabatino, G., Quartieri, S., Barbieri, R., Cavalazzi, B., Ferretti, A., Danovaro, R., Romeo, T., Andaloro, F., Esposito, V., Scotti, G., Tripodo, A. & Italiano, F. 2021. Rolling Ironstones from Earth and Mars:

Terrestrial Hydrothermal Ooids as a Potential Analogue of Martian Spherules. *Minerals 11*, 460. DOI 10.3390/min11050460

Dunn, K.A., Mclean, R.J.C., Upchurch, G.R. & Folk, R.L. 1997. Enhancement of leaf fossilization potential by bacterial biofilms. *Geology 25*, 1119–1122. DOI 10.1130/0091-7613(1997)025<1119:EOLFPB>2.3.CO;2

Effenberger, H., Mereiter, K. & Zemann, J. 1981. Crystal structure refinements of magnesite, calcite, rhodochrosite, siderite, smithsonite, and dolomite, with discussion of some aspects of the stereochemistry of calcite type carbonates. *Zeitschrift für Kristallographie – Crystalline Materials 156*, 233–243. DOI 10.1524/zkri.1981.156.3-4.233

Feist, R. & Schönlaub, H.-P. 1974. Zur Silur/Devon-Grenze in der östlichen Montagne Noire (Südfrankreich). *Neues Jahrbuch für Geologie und Paläontologie, Monatshefte 4*, 200–219.

Feng, Q., Liu, Z.H. & Ooi, K. 2008. Birnessite-type Manganese Oxide by Redox Precipitation, 1–6. *In* Schubert, U., Hüsing, N. & Laine, R.M. (eds) *Materials Syntheses*. Springer, Vienna. DOI 10.1007/978-3-211-75125-1_8

Ferretti, A. 2005. Ooidal ironstones and laminated ferruginous deposits from the Silurian of the Carnic Alps, Austria. *Bollettino della Società Paleontologica Italiana 44*, 263–278.

Ferretti, A. & Kříž, J. 1995. Cephalopod Limestone Biofacies in the Silurian of the Prague Basin, Bohemia. *Palaios 10*, 240–253. DOI 10.2307/3515255

Ferretti, A. & Serpagli, E. 1999. Geological outline, community sequence and paleoecology of the Silurian of Sardinia. *Rivista Italiana di Paleontologia e Stratigrafia 102*, 353–362.

Ferretti, A., Corradini, C. & Serpagli, E. 1998. The Silurian and Devonian sequence in SW Sardinia. *Giornale di Geologia 60*, 57–61.

Ferretti, A., Cavalazzi, B., Barbieri, R., Westall, F., Foucher, F. & Todesco, R. 2012. From black-and-white to colour in the Silurian. *Palaeogeography, Palaeoclimatology, Palaeoecology 367–368*, 178–192. DOI 10.1016/j.palaeo.2012.10.025

Ferretti, A., Foucher, F., Westall, F., Medici, L. & Cavalazzi, B. 2023a. Ferruginous biolaminations within the pre-Hirnantian (Late Ordovician) of the Carnic Alps, Austria. *Geobios 81*, 167–177. DOI 10.1016/j.geobios.2023.01.007

Ferretti, A., Schönlaub, H.P., Sachanski, V., Bagnoli, G., Serpagli, E., Vai, G.B., Yanev, S., Radonjić, M., Balica, C., Bianchini, L., Colmenar, J. & Gutiérrez-Marco, J.C. 2023b. A global view on the Ordovician stratigraphy of south-eastern Europe, 465–499. *In* Harper, D.A.T., Lefebvre, B., Percival, I.G. & Servais, T. (eds) *A Global Synthesis of the Ordovician System: Part 1. Geological Society London, Special Publication 532*. DOI 10.1144/SP532-2022-174

Foucher, F. 2021. Influence of laser shape on thermal increase during micro-Raman spectroscopy analyses. *Journal of Raman Spectroscopy 53*, 163–180. DOI 10.1002/jrs.6230

Frezzotti, M.L., Tecce, F. & Casagli, A. 2012. Raman spectroscopy for fluid inclusion analysis. *Journal of Geochemical Exploration 112*, 1–20. DOI 10.1016/j.gexplo.2011.09.009

Gámez Vintaned, J.A., Liñán, E. & Zhuravlev, A.Y. 2011. A New Early Cambrian Lobopod-Bearing Animal (Murero, Spain) and the Problem of the Ecdysozoan Early Diversification, 193–219. *In* Pontarotti, P. (ed.) *Evolutionary Biology – Concepts, Biodiversity, Macroevolution and Genome Evolution*. Springer, Berlin & Heidelberg. DOI 10.1007/978-3-642-20763-1_12

Gehling, J.G. 1999. Microbial Mats in Terminal Proterozoic Siliciclastics: Ediacaran Death Masks. *Palaios 14*, 40–57. DOI 10.2307/3515360

Gnoli, M. & Histon, K. 1998. Silurian nautiloid Cephalopods from the Carnic Alps: a preliminary investigation. *Bollettino della Società Paleontologica Italiana 36*, 311–330.

Gnoli, M., Histon, K. & Serventi, P. 2000. Revision of Silurian cephalopods from the Carnic Alps: The Gortani and Vinassa de Regny collection, 1909. *Bollettino della Società Paleontologica Italiana 39*, 3–12.

Gualtieri, A.F., Gatta, G.D., Arletti, R., Artioli, G., Ballirano, P., Cruciani, G., Guagliardi, A., Malferrari, D., Masciocchi, N. & Scardi, P. 2019. Quantitative phase analysis using the Rietveld method: towards a procedure for checking the reliability and quality of the results. *Periodico di Mineralogia 88*, 147–151. DOI 10.2451/2019PM870

Gutiérrez-Marco, J.C., Robardet, M. & Piçarra, J.M. 1998. Silurian stratigraphy and paleogeography of the Iberian Peninsula (Spain and Portugal), 13–44. *In* Gutiérrez-Marco, J.C. & Rábano, I. (eds) *Proceedings of the 6th International Graptolite Conference of the GWG (IPA) and the 1998 Field Meeting of the International Subcommission on Silurian Stratigraphy (ICS-IUGS). Temas Geológico–Mineros ITGE 23.*

Gutiérrez-Marco, J.C., Sarmiento, G.N., Robardet, M., Rábano, I. & Vaněk, J. 2001. Upper Silurian fossils of bohemian type from NW Spain and their palaeogeographical significance. *Journal of the Czech Geological Society 46(3–4)*, 247–258.

Hazemann, J.-L., Bérar, J.F. & Manceau, A. 1991. Rietveld studies of the aluminium-iron substitution in synthetic goethite. *Materials Science Forum 79–82*, 821–826. DOI 10.4028/www.scientific.net/MSF.79-82.821

Heritsch, F. 1929. Faunen aus dem Silur der Ostalpen. *Abhandlungen der Geologischen Bundesanstalt 23*, 1–183.

Hillier, S. 1994. Pore-lining chlorites in sandstones: potential for misidentification as early diagenetic cement. *Clay Minerals 29(4)*, 665–670. DOI 10.1180/claymin.1994.029.4.20

Histon, K. 1999. Revision of Silurian Nautiloid Cephalopods from the Carnic Alps (Austria) – The Heritsch (1929) Collection in the Geological Survey of Austria. *Abhandlungen der Geologischen Bundesanstalt 56*, 229–258.

Histon, K. 2012. The Silurian nautiloid-bearing strata of the Cellon Section (Carnic Alps, Austria): Color variation related to events. *Palaeogeography, Palaeoclimatology, Palaeoecology 367–368*, 231–255. DOI 10.1016/j.palaeo.2012.10.012

Jaeger, H. 1975. Die Graptolithenführung im Silur/Devon des Cellon-Profils (Karnische Alpen). *Carinthia II 85*, 111–126.

Jaeger, H. & Schönlaub, H.P. 1980. Silur und Devon nördlich der Gundersheimer Alm in den Karnischen Alpen (Österreich). *Carinthia II 90*, 403–444.

Jaeger, H. & Schönlaub, H.P. 1994. "Graptolithengraben" (graptolite gorge) north of Upper Bischofalm. *Berichte der Geologischen Bundesanstalt 30*, 97–100.

Jarochowska, E., Tonarová, P., Munnecke, A., Ferrová, L., Sklenář, J. & Vodrážková, S. 2013. An acid-free method of microfossil extraction from clay-rich lithologies using the surfactant Rewoquat. *Palaeontologia Electronica 16*, 1–16. DOI 10.26879/382

Kihara, K. 1990. An X-ray study of the temperature dependence of the quartz structure. *European Journal of Mineralogy 2*, 63–77. DOI 10.1127/ejm/2/1/0063

Kříž, J. 1999. Silurian and lowermost Devonian bivalves of bohemian type from the Carnic Alps. *Abhandlungen der Geologischen Bundesanstalt 56*, 259–316.

Kříž, J. 2006. Bohemian type bivalves *Praeostrea bohemica* Barrande, 1881 and *Slavinka plicata* (Barrande, 1881) from the Silurian and earliest Devonian of the Carnic Alps (Austria). *Bulletin of Geosciences 81*, 147–149. DOI 10.3140/bull.geosci.2006.02.147

Lanson, B., Drits, V.A., Feng, Q. & Manceau, A. 2002. Structure of synthetic Na-birnessite: Evidence for a triclinic one-layer unit cell. *American Mineralogist 87*, 1662–1671. DOI 10.2138/am-2002-11-1215

Locatelli, E.R., McMahon, S. & Bilger, H. 2017. Biofilms mediate the preservation of leaf adpression fossils by clays. *Palaios 32*, 708–724. DOI 10.2110/palo.2017.043

Luan, X., Sproat, C.D., Jin, J. & Zhan, R. 2024. Depositional environments, hematite–chamosite differentiation and origins of Middle Ordovician iron ooids in the Upper Yangtze region, South China. *Sedimentology 71*, 2210–2247. DOI 10.1111/sed.13213

Matheson, E.J., Pufahl, P.K., Voinot, A., Murphy, J.B. & Fitzgerald, D.M. 2022. Ironstone as a proxy of Paleozoic ocean oxygenation. *Earth and Planetary Science Letters 594*, 117715. DOI 10.1016/j.epsl.2022.117715

Mozley, P.S. & Wersin, P. 1992. Isotopic composition of siderite as an indicator of depositional environment. *Sedimentology 39*, 1119–1136. DOI 10.1130/0091-7613(1992)020<0817:ICOSAA>2.3.CO;2

Mücke, A. 2006. Chamosite, siderite and the environmental conditions of their formation in chamosite-type Phanerozoic ooidal ironstones. *Ore Geology Reviews 28*, 235–249. DOI 10.1016/j.oregeorev.2005.03.004

Papadopoulos, V., Tsikos, H., Boyce, A.J. & Mark, D.F. 2019. Regional isotopic fingerprinting of hydrothermal barite mineralisation and its possible association to epigenetic Fe and Mn ore formation in the Paleoproterozoic Transvaal Supergroup of South Africa. *Applied Earth Science 128*, 57. DOI 10.1080/25726838.2019.1607158

Papazzoni, C.A., Cavalazzi, B., Brigatti, M.F., Filipescu, S., Foucher, F., Medici, L., Westall, F. & Ferretti, A. 2022. The significance of iron ooids from the middle Eocene of the Transylvanian Basin, Romania. *Gondwana Research 111*, 64–75. DOI 10.1016/j.gr.2022.06.003

Post, J.E. 1999. Manganese oxide minerals: Crystal structures and economic and environmental significance. *PNAS 96*, 3447–3454. DOI 10.1073/pnas.96.7.3447

Raiswell, R. & Canfield, D.E. 2012. The iron biogeochemical cycle past and present. *Geochemical Perspectives 1*, 1–220. DOI 10.7185/geochempersp.1.1

Rddad, L. 2017 Fixation and redistribution of arsenic during early and late diagenesis in the organic matter-rich members of the Lockatong formation, Newark basin, USA: Implications for the quality of groundwater. *Atlantic Geology 53*, 253–268. DOI 10.4138/atlgeol.2017.010

Retallack, G.J. 2022. Ferruginous biofilm preservation of *Ediacaran* fossils. *Gondwana Research 110*, 73–89. DOI 10.1016/j.gr.2022.06.007

Rudmin, M., Banerjee, S., Abdullayev, E., Ruban, A., Filimonenko, E., Lyapina, E., Kashapov, R. & Mazurov, A. 2020. Ooidal ironstones in the Meso-Cenozoic sequences in western Siberia: assessment of formation processes and relationship with regional and global earth processes. *Journal of Palaeogeography 9*, 1. DOI 10.1186/s42501-019-0049-z

Rudmin, M., Banerjee, S., Maximov, P., Novoselov, A., Trubin, Y., Smirnov, P., Abersteiner, A., Tang, D. & Mazurov, A. 2022. Origin of ooids, peloids and micro-oncoids of marine ironstone deposits in Western Siberia (Russia). *Journal of Asian Earth Sciences 237*, 105361. DOI 10.1016/j.jseaes.2022.105361

Schönlaub, H.P. 1997. The Silurian of Austria. *Berichte der Geologischen Bundsanstalt 40*, 20–41.

Schönlaub, H.P. 1998. The Ordovician-Silurian boundary in the Carnic Alps of Austria. *Bulletin of the British Museum (Natural History) Geology 43*, 95–100.

Schwark, L., Ferretti, A., Papazzoni, C.A. & Trevisani, E. 2009. Organic geochemistry and paleoenvironment of the Early Eocene "Pesciara di Bolca" Konservat-Lagerstätte, Italy. *Palaeogeography, Palaeoclimatology, Palaeoecology 273*, 272–285. DOI 10.1016/j.palaeo.2008.03.009

Serventi, P. 2001. *Cefalopodi nautiloidei del Siluriano delle Alpi Carniche*. 145 pp. Ph.D. Thesis, Università degli Studi di Modena e Reggio Emilia, Italy.

Serventi, P. & Gnoli, M., 2000. Nuovi ritrovamenti di Cefalopodi nautiloidei nelle Alpi Carniche. *Giornale di Geologia 3, Suppl.*, 9–14.

Serventi, P., Gnoli, M. & Histon, K. 2000. Revisione di Cefalopodi nautiloidei siluriani delle Alpi Carniche provenienti da collezioni storiche. *Accademia Nazionale di Scienze Lettere e Arti di Modena 21*, 227–230.

Serventi, P., Corradini, C., Simonetto, L. & Pondrelli, M. 2007. Cefalopodi nautiloidei Siluriani del Museo Friulano di Storia Naturale. *Gortania 28*, 9–57.

Serventi, P., Gnoli, M. & Simonetto, L. 2010. Actinocerid cephalopods from the Silurian of the Carnic Alps (Italian side). *Bollettino della Società Paleontologica Italiana 49*, 75–81.

Spicer, R.A. 1977. The pre-depositional formation of some leaf impressions. *Palaeontology 20*, 907–912.

Štorch, P. 2023. Graptolite biostratigraphy and biodiversity dynamics in the Silurian System of the Prague Synform (Barrandian area, Czech Republic). *Bulletin of Geosciences 98*, 1–78. DOI 10.3140/bull.geosci.1862

Štorch, P. & Feist, R. 2008. Lowermost Silurian graptolites of Montagne Noire, France. *Journal of Paleontology 82,* 938–956. DOI 10.1666/07-004.1

Tang, D., Shi, X., Jiang, G., Zhou, X. & Shi, Q. 2017. Ferruginous seawater facilitates the transformation of glauconite to chamosite: An example from the Mesoproterozoic xiamaling formation of North China. *American Mineralogist 102*, 2317–2332. DOI 10.2138/am-2017-6136

Tebo, B.M., Bargar, J.R., Clement, B.G., Dick, G.J., Murray, K.J., Parker, D., Verity, R. & Webb, S.M. 2004. Biogenic manganese oxides: properties and mechanisms of formation. *Annual Review of Earth and Planetary Sciences 32*, 287–328. DOI 10.1146/annurev.earth.32.101802.120213

Walker, J.R. & Bish, D.L. 1992. Application of Rietveld refinement techniques to a disordered II*b* Mg-chamosite. *Clays and Clay Minerals 40*, 319–322. DOI 10.1346/CCMN.1992.0400311

Walliser, O. 1964. Conodonten des Silurs. *Abhandlungen des Hessischen Landesamtes für Bodenforschung zu Wiesbaden 41*, 1–106.

Wan, B., Chen, Z., Yuan, X., Pang, K., Tang, Q., Guan, C., Wang, X., Pandey, S.K., Droser, M.L. & Xiao, S. 2020. A tale of three taphonomic modes: The Ediacaran fossil *Flabellophyton* preserved in limestone, black shale, and sandstone. *Gondwana Research 84*, 296–314. DOI 10.1016/j.gr.2020.04.003

Worden, R.H., Griffiths, J., Wooldridge, L.J., Utley, J.E.P., Lawan, A.Y., Muhammed, M.D., Simon, N. & Armitage, P.J. 2020. Chlorite in sandstones. *Earth-Science Reviews 204*, 103105. DOI 10.1016/j.earscirev.2020.103105

Young, H.D. 1962. *Statistical Treatment of Experimental Data*. 172 pp. McGraw-Hill Book Company, New York, NY, USA.